Journal of Power Sources 216 (2012) 508–514

Contents lists available at SciVerse ScienceDirect

Journal of Power Sources

journal homepage: www.elsevier.com/locate/jpowsour

In-situ synthetize multi-walled carbon nanotubes@MnO_2 nanoflake core–shell structured materials for supercapacitors

Huajun Zheng [a,b,*], Jiaoxia Wang [a], Yi Jia [c], Chun'an Ma [a,b]

[a] Department of Applied chemistry, Zhejiang University of Technology, Hangzhou 310032, China
[b] State Key Laboratory Breeding Base of Green Chemistry Synthesis Technology, Zhejiang University of Technology, Hangzhou 310032, China
[c] ARC Centre of Excellence for Functional Nanomaterials, School of engineering and AIBN, The University of Queensland, St. Lucia, Brisbane, QLD 4072, Australia

HIGHLIGHTS

- A facile in-situ co-precipitation method is developed to synthesize the MWCNTs@MnO_2 core–shell structured material.
- Birnessite-type MnO_2 nanoflakes chemically grew around the surface of the MWCNTs.
- The material had the high specific capacitance (380 F g^{-1}) and power density (11.28 kW kg^{-1}).
- The material showed excellent capacitance retention (82.7%) after 3500 cycles.

GRAPHICAL ABSTRACT

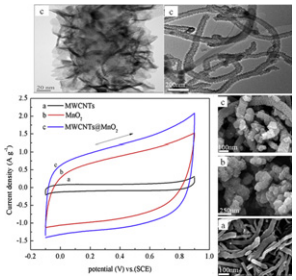

ARTICLE INFO

Article history:
Received 19 February 2012
Received in revised form
5 June 2012
Accepted 6 June 2012
Available online 21 June 2012

Keywords:
Supercapacitor
Manganese dioxide nanoflake
Carbon nanotube
Core–shell structure

ABSTRACT

A new type of core–shell structured material consisting of multi-walled carbon nanotubes (MWCNTs) and manganese dioxide (MnO_2) nanoflake is synthesized using an in-situ co-precipitation method. By scanning electron microscopy and transition electron microscope, it is confirmed that the core–shell nanostructure is formed by the uniform incorporation of birnessite-type MnO_2 nanoflake growth round the surface of the activated-MWCNTs. That core–shell structured material electrode presents excellent electrochemical capacitance properties with the specific capacitance reaching 380 F g^{-1} at the current density of 5 A g^{-1} in 0.5 M Na_2SO_4 electrolyte. In addition, the electrode also exhibits good performance (the power density: 11.28 kW kg^{-1} at 5 A g^{-1}) and long-term cycling stability (retaining 82.7% of its initial capacitance after 3500 cycles at 5 A g^{-1}). It mainly attributes to MWCNTs not only providing considerable specific surface area for high mass loading of MnO_2 nanoflakes to ensure effective utilization of MnO_2 nanoflake, but also offering an electron pathway to improve electrical conductivity of the electrode materials. It is clearly indicated that such core–shell structured materials including MWCNTs and MnO_2 nanoflake may find important applications for supercapacitors.

1. Introduction

Supercapacitors, also known as electrochemical capacitors, have attracted tremendous attention due to its high power density and long-term cycles [1]. Generally, they can be classified into two categories in terms of the energy storage mechanism, i.e., electric double layer capacitors (EDLCs) and pseudo-capacitors [2]. As usual, activated carbons with high surface areas are used as electrode materials for EDLCs and transition-metal oxides are used as electrode materials for the pseudo-capacitors related to the redox reaction [3–6], respectively. Ruthenium oxide (RuO_2) has exhibited prominent capacitive properties as a supercapacitor electrode material, up to 760 F g^{-1} in aqueous electrolytes. But its high

* Corresponding author. State Key Laboratory Breeding Base of Green Chemistry Synthesis Technology, Zhejiang University of Technology, Hangzhou 310032, China. Tel.: +86 571 88320037; fax: +86 571 88320272.
E-mail address: zhenghj@zjut.edu.cn (H. Zheng).

0378-7753/$ – see front matter
http://dx.doi.org/10.1016/j.jpowsour.2012.06.047

production cost will exclude it from commercial applications [7]. Manganese dioxide (MnO_2) is a promising electrode material for pseudo-capacitors in replacing RuO_2 due to low cost and little toxicity [8]. Toupin and Brousse predicted theoretically a high specific capacitance (SC) of 1370 F g^{-1} for MnO_2-based supercapacitor electrodes based on each of Mn atom utilized for energy-storage [9]. However, the practical capacitance of MnO_2 materials is far lower than their theoretical SC because of their intrinsically poor electronic conductivity and densely packed structure [10–13]. One key solution to utilize Mn atom effectively in energy-storage is designing and controlling the morphology and crystallography of manganese oxides at nanoscale. A number of studies have been reported that a capacitance value of nanoscale manganese oxides can be improved by enhancing the surface area [14,15]. Ming and Li have successfully synthesized a birnessite-type MnO_2 nanosphere with 70–90 nm in diameter and a large specific surface area of 213.6 m^2 g^{-1} and this nanosphere exhibits an improved SC of 210 F g^{-1} at 0.2 A g^{-1} in 1.0 M Na_2SO_4 electrolyte [16].

Another strategy to improve the electronic conductivity is to synthesize manganese oxide composites with conductive materials. Actually, carbonaceous materials with good electronic conductivity have attracted considerable attention in recent years [17–19]. Undoubtedly, carbon nanotube (CNT) is an ideal optional material because CNT has several remarkable characteristics making them particularly attractive for supercapacitors, such as excellent electrical conductivity, good chemical stability, strong mechanical property and a high electrochemically accessible area. Many different approaches have been developed in this area of coating MnO_2 on CNTs to make the best of both the excellent electrical conductivity of CNTs and the high SC of MnO_2. Recently, Jiang and Huang obtained poorly crystallined α-MnO_2 grown on multi-walled carbon nanotubes (MWCNTs) by reducing $KMnO_4$ in ethanol. The composite gave the SC of 179 F g^{-1} at a scan rate of 5 mV s^{-1} and remained 114.6 F g^{-1} at 100 mV s^{-1} [20]. Wang and Peng synthesized MnO_2/CNTs by a facile direct redox reaction between potassium permanganate ($KMnO_4$) and CNTs without any other oxidant or reductant addition. The composite kept 90% of its SC after 2000 cycles at the current density of 5 A g^{-1} [21]. Similar approach was also demonstrated by Ma and his co-workers. The SC of the obtained MnO_2/CNTs composite reached 250 F g^{-1} and the SC of MnO_2 in the composite was as high as 580 F g^{-1} at the current density of 1 A g^{-1} [22]. Raymundo-Pinero and Khomenko prepared CNTs/MnO_2 electrode by a physical mixing method and studied different aqueous electrolytic solutions with pH value 6.4 and 10 [23]. Fan and Chen prepared γ-MnO_2/ACNT (well-aligned carbon nanotube arrays) by electrochemically induced deposition method with excellent capacitance performance both on γ-MnO_2 and the composite [24]. In previous work, we assembled MWCNTs and MnO_2 nanosheets by an electrostatic layer-by-layer assembly technique and also obtained good electrochemical performance [25]. Chou and Wang electrodeposited MnO_2 nanowires onto the surface of CNTs paper by a cyclic voltammetric technique and the MnO_2/CNT electrode displayed the SC of 167.5 F g^{-1} at 0.077 A g^{-1} [26]. Teng and Santhanagopalan prepared the three-dimensional MnO_2/CNT electrode by a one-pot hydrothermal method with showing that the hydrothermally mixed electrode yielded a higher SC than the mechanically mixed electrode [27]. Similar hydrothermal method was also applied by Tang and his co-workers and the electrode had an excellent rate capability and delivered an energy density of 17.8 Wh kg^{-1} at 400 W kg^{-1} [28].

Recently, we have demonstrated an improved electrochemical behavior of the sandwiched film of MnO_2 nanosheet and multi-walled carbon nanotube (MWCNT) by using the layer-by-layer method [29]. Multilayer films consisting of MWCNTs and Cobalt oxyhydroxide nanoflakes are also developed by interchangeable electrostatic self-assembly and electrodeposition technique, and experimental studies reveal that those films present excellent electrochemical capacitance being 389 F g^{-1} [30]. The overall improved electrochemical properties are taken into account for the micro-porous nanostructure, large specific surface area and good electrical conductance. In the present work, our strategy in designing a core–shell structured materials containing of MWCNTs and homogeneous MnO_2 nanoflake (MWCNTs@MnO_2) were facile synthesized under in-situ co-precipitation method. Fig. 1 schematically outlines the synthesis procedures of MWCNTs@MnO_2. For the redox deposition, potassium permanganate ($KMnO_4$) can be reduced spontaneously to MnO_2 by oxidizing manganese sulfate ($MnSO_4$) in neutral solution at room temperature [31]. The redox reaction can be written as follows:

$$3MnSO_4 + 2KMnO_4 + 2H_2O = 5MnO_2 + 2H_2SO_4 + K_2SO_4$$

The activated-MWCNTs acted as cores provide rough substrate with a large surface area for the formation of MnO_2 nanoflakes. The thin and homogeneous MnO_2 nanoflakes growing around the surface of MWCNTs significantly improve the electrochemical utilization of the birnessite-MnO_2. Furthermore, MWCNTs also offer a facile electron pathway to enhance the electronic conductivity of electrode materials.

2. Experimental

2.1. Preparation of MWCNTs@MnO_2

MWCNTs were purchased from Nanotech Port Co., Ltd. (Shenzhen, China), with a diameter of 30–60 nm and length of 5–15 μm. Titanium foil was purchased from CSG Holding Co., Ltd. (Shenzhen, China), The reagents and electrolytes, $MnSO_4 \cdot H_2O$, $KMnO_4$, and Na_2SO_4 were purchased from Aldrich and used without further purification. All other chemicals and solvents were of analytical grade. Deionized (DI) water was used in all aqueous solutions.

The initial MWCNTs were activated by stirring in 65 wt% nitric acid at 25 °C for 24 h [21]. After stirring, the activated-MWCNTs (a-

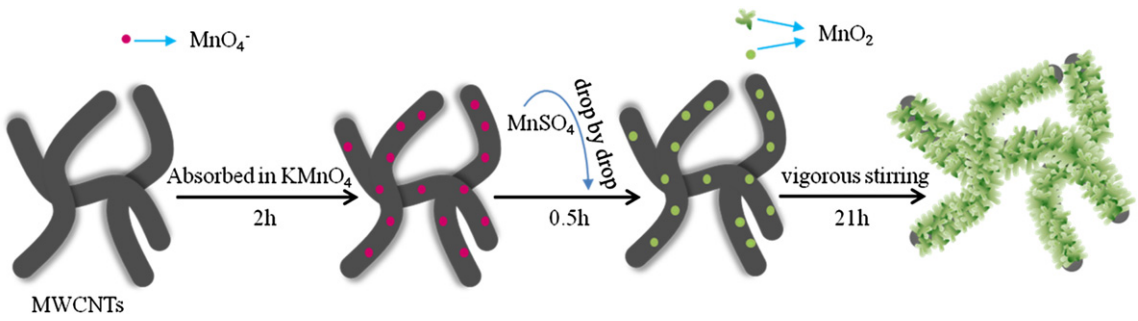

Fig. 1. Schematic illustration for the growth process of MWCNTs@MnO_2.

MWCNTs) were obtained by rinsing with deionized water and drying in the air at 100 °C. The typical synthesis process of the MWCNTs@MnO_2 composite can be described as follows. Firstly, 0.15 g of a-MWCNTs was dispersed into 80 ml 0.10 M $KMnO_4$ solution under stirring at 40 °C for 2 h. Subsequently, 20 ml 0.20 M $MnSO_4$ solution was added dropwise into the above suspension with vigorous stirring. After that, the reaction mixture was kept at 40 °C for 21 h. Finally, the suspension was filtered, washed several times with deionized water and alcohol, and the filter cake was dried in an oven at 120 °C for 6 h. The resulting brown powders were collected. For comparison, the pristine MnO_2 materials were also synthesized by following precisely the above-mentioned process without a-MWCNTs.

2.2. Characterization of structure and morphology

Powder X-ray diffraction (XRD) patterns of samples were obtained by using a TW3040/60 diffractometer (Tanalygical Company, Holland) in which Cu-Kα ($\lambda = 0.154$ nm) was used as the radiation source. The samples were analyzed by a thermogravimetric analyzer (Model Perkin–Elmer TGA-7) to determine the relative content of a-MWCNTs. The morphologies of the samples were examined by a Hitachi S-4800 scanning electron microscopy (SEM) and a transition electron microscope (TEM, Tecnai G2 F30 FEI Inc. Holland). The pore size distribution and surface area of the samples were determined by nitrogen adsorption at −196 °C with an automated adsorption apparatus (Micromeritics ASAP 2020). The pore size distribution was determined by the BJH method from the desorption isotherm. The surface area was derived from the Brunauer–Emmett–Teller (BET) equation [32].

2.3. Electrochemical measurements

The electrode was prepared by mixing 80 wt% active material, 15 wt% acetylene black (Timcal) and 5 wt% polyvinylidene fluoride (PVDF) (Fluka) in 1-methyl-2-pyrrolidinone (Aldrich) and coated onto titanium foil current collector (1 cm × 1 cm) using a blade. The electrode was dried at 100 °C for 6 h to evaporate solvent. Both the three-electrode and symmetric cell configurations were employed. The former used a platinum gauze electrode and saturated calomel electrode (SCE) as counter electrode and reference electrode, respectively. The symmetric cell included two identical electrodes placed face to face with a separator in between. Cyclic voltammetry (CV), galvanostatic charge–discharge, cycle life and electrochemical impedance spectroscopy (EIS) measurements were performed with an EG&G 273A potentiostat in 0.5 M Na_2SO_4 electrolyte at room temperature. It is to be noted that CV and EIS measurements work with the three-electrode cell configuration, while the galvanostatic charge–discharge and cycle life tests used the symmetric cell configuration.

The average specific capacitance (C, F g^{-1}) from the CV curves is calculated according to the following integral Eq. (1). The average specific capacitance (C, F g^{-1}), and power density (P, kW kg^{-1}), from the charge/discharge curves can be calculated based on Eqs. (2) and (3).

$$C = \frac{1}{m \cdot \upsilon \cdot \Delta V} \int I_{(V)} \mathrm{d}V \tag{1}$$

$$C = \frac{2I \cdot \Delta t}{m \cdot \Delta V} \tag{2}$$

$$P = \frac{(\Delta V)^2}{4m \cdot R} \tag{3}$$

Here, m (g) is the active material mass of one electrode, υ (mV s^{-1}) is the potential scan rate, ΔV (V) is the sweep potential window and $I_{(V)}$ (A) is the voltammetric current on CV curves, I (A) is the applied current, Δt (s) is the discharge time, R (Ω) is the effective series resistance and estimated using the voltage drop at the beginning of the discharge.

3. Results and discussion

3.1. Chemistry composition and micro morphology of the materials

Fig. 2 shows the XRD patterns of a-MWCNTs and MWCNTs@MnO_2. As shown in Fig. 2a, the diffraction peaks at 2θ values of 26.16°, 44.32° can be well assigned to the (002) and (101) planes of graphite carbon [33]. This significant photoemission is a typical characteristic of a-MWCNTs. There are three diffraction peaks at 12.54°, 37.19° and 65.71° of 2θ reflected in Fig. 2b, which can be perfectly indexed as (001), (111) and (020) planes of birnessite-type MnO_2 (JCPDS 42-1317, δ-MnO_2) [34,35]. Furthermore, from Fig. 2b, the peak at 26.16° becomes weak and the peak at 44.32° of 2θ has disappeared simultaneously, indicating that the synthesized MnO_2 nanoflakes were deposited uniformly on the surface of MWCNTs. This phenomenon has also been confirmed by the SEM images of the composite given in Fig. 3, which displays a homogeneous MWCNTs@MnO_2 core–shell structure. From Fig. 3, the whole surface of MWCNTs is almost completely covered by the nanoflakes of MnO_2. The generated MWCNTs@MnO_2 did not show any reunion phenomenon and each MWCNTs@MnO_2 is about 100 nm in diameter, indicating the nanoflake thickness of MnO_2 is about 20 nm.

Typical TEM micrographs of the MWCNTs@MnO_2 were given in Fig. 4a, c and d. As demonstrated in Fig. 4a, the obtained MWCNTs@MnO_2 core–shell structured material is about 2.0–2.5 μm in length and shows fine dispersion. Energy dispersive X-ray spectrum (in Fig. 4b) reveals that the MWCNTs@MnO_2 materials are mainly composed of C which can be explained by the results of XRD patterns (in Fig. 2b, the (002) plane is of graphite carbon), Mn, O and K elements (here the Cu element is from the Cu grid), suggesting the synthesized MnO_2 is K-birnessite. Fig. 4c is the low-magnification TEM image of MWCNTs@MnO_2, showing that the MnO_2 nanoflakes indeed chemically grow around the surface of MWCNT rather than physically covering it. Fig. 4d is the high-resolution transition electron microscope (HRTEM) magnified by the circled section (Fig. 4c), which indicates three typical interlayer spacing of 0.35, 0.25 and 0.24 nm, respectively. These interlayer spacing correspond to the (002), (201) and the (111) planes of the monoclinic-structured δ-MnO_2, conforming the results shown in Fig. 2b.

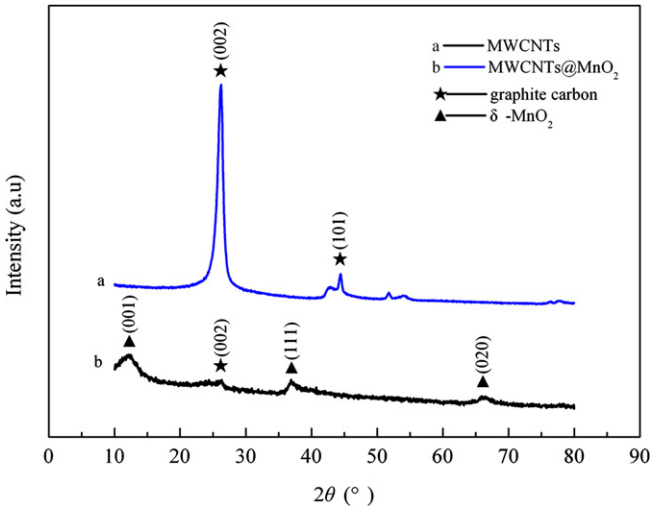

Fig. 2. XRD patterns of MWCNTs (a) and MWCNTs@MnO_2 (b).

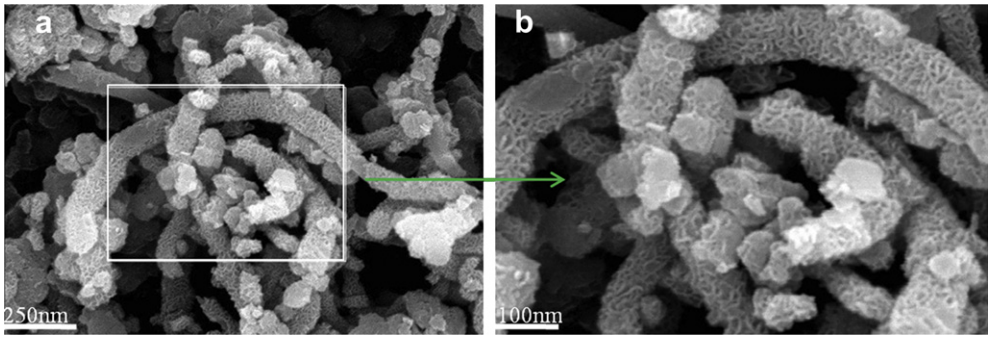

Fig. 3. SEM images of MWCNTs@MnO_2.

3.2. Percentage content of MWCNTs in MWCNTs@MnO_2

The thermogravimetric analysis (TGA) and differential thermogravimetric analysis (DTA) curves for MWCNTs@MnO_2 composite were shown in Fig. 5, which exhibit three well-defined steps. The 16.7% weight loss between 30 and 180 °C is attributed to the release of hydration water in the composite. The subsequent weight loss of 6.6% between 330 and 460 °C is due to the burning of MWNTs, in accordance with the DTA curve. In addition, the final weight loss of ~2% between 620 and 700 °C is assigned to the transformation of MnO_2 to Mn_3O_4. Therefore, the content of MWCNTs in the composite is 6.6%.

3.3. Pore structure and specific surface area of MWCNTs@MnO_2

The porosity of the generated MWCNTs@MnO_2 material was reflected in BJH curves, shown in Fig. 6. A very broad distribution ranging from 31 to 43 nm with a peak at 38 nm can be found in the mesopores region. Taking into account that this value is between the MWCNTs diameter, 30–60 nm, the mesoporous system must have resulted from the inner pores of the individual MWCNTs. Moreover, according to the TEM images, there are no pores inside each nanoflake of MnO_2, thus it can be inferred that the mesopores between 20 and 25 nm are mainly derived from the voids among different flakes of the growth MnO_2. The pore volume is found to be 0.116 $cm^3\ g^{-1}$. Such polyporous MWCNTs@MnO_2 material is likely to the benefit of a rapid diffusion of electrolyte and ions. The BET surface area of the MWCNTs@MnO_2 was characterized by N_2 adsorption/desorption isotherm in Fig. 6 (the inset). It is obvious that a typical type IV isotherm with a hysteresis loop appears in the N_2 adsorption/desorption isotherm for relative pressure (P/P_0) range between 0.5 and 0.99, indicating the disordered mesoporous structure [15]. The specific surface area was calculated by BET

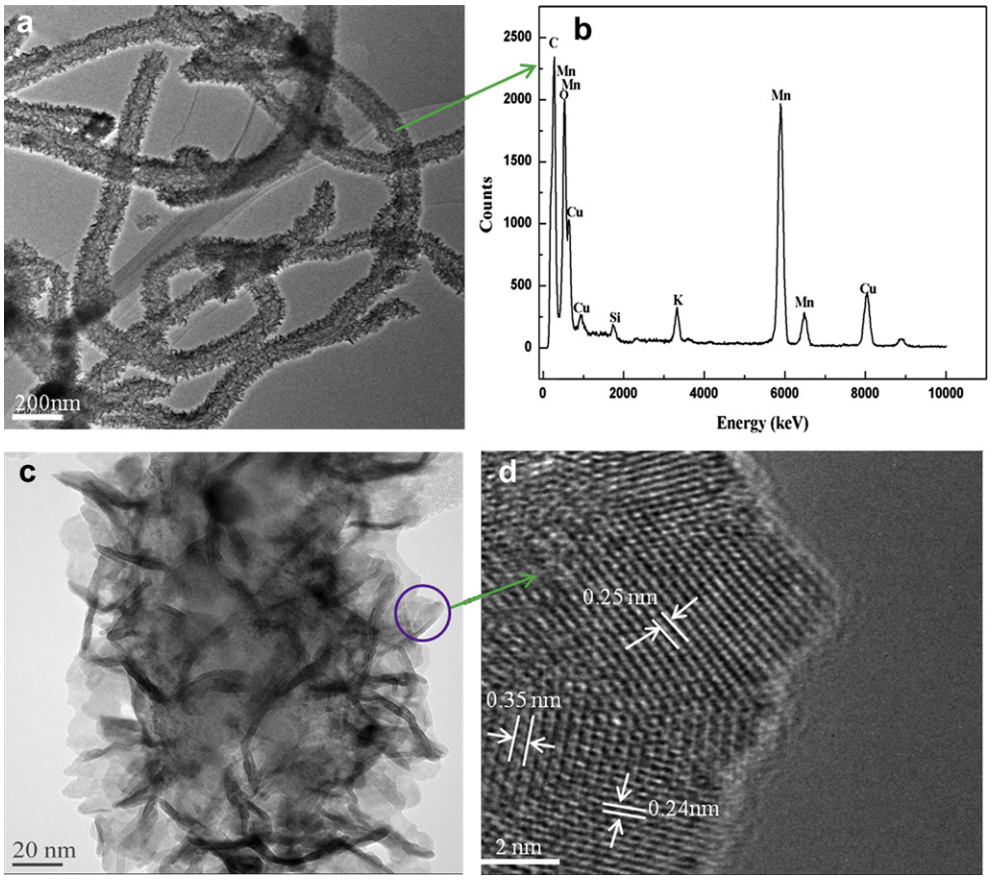

Fig. 4. TEM images of MWCNTs@MnO_2 (a, c); HR-TEM image of synthesized MnO_2 nanoflake (d); the energy dispersive X-ray spectrum of the MWCNTs@MnO_2 (b).

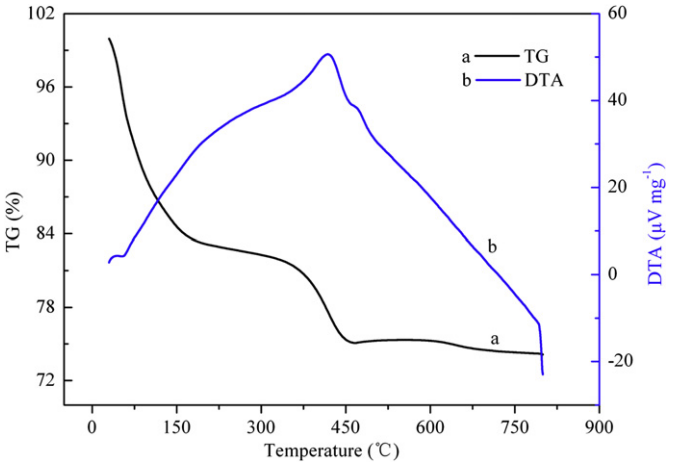

Fig. 5. TG/DTA curves of MWCNTs@MnO_2.

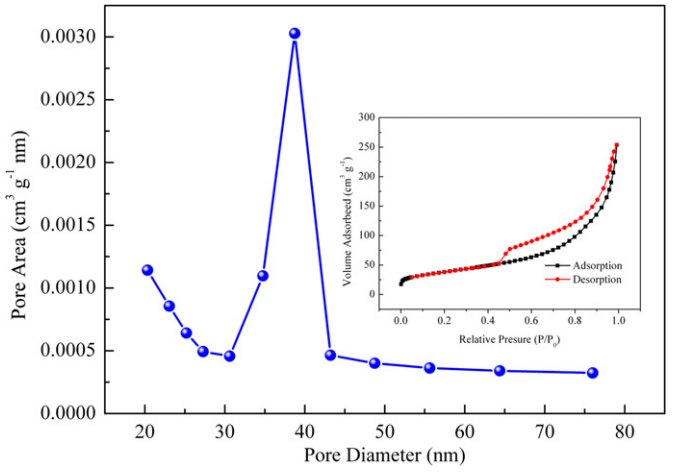

Fig. 6. Pore size distribution and (the inset) N_2 adsorption–desorption isotherms of MWCNTs@MnO_2.

equation and the MWCNTs@MnO_2 gives a high specific surface of 135.54 $m^2\ g^{-1}$ [19]. The large BET surface area will enable the extended interface area with the surface adsorption/desorption of protons or alkali cations between active materials and electrolytes.

3.4. Electrical conductivity of the pristine MnO_2, MWCNTs and MWCNTs@MnO_2

CV measurements were conducted for the three samples as recorded at a 5 mV s^{-1} scan rate, shown in Fig. 7. The right insets of SEM images are corresponding to the curves: (a) MWCNTs, (b) pristine MnO_2, (c) MWCNTs@MnO_2, respectively. Curve (a) exhibits a fairly rectangular shape, which implies a typical feature of the electric double layer capacitance and gets the SC of 28 F g^{-1} from Eq. (1). Curve (b), by contrast, demonstrates a much larger capacitance, mainly because the pristine MnO_2 with nanostructure and high BET surface area (56.79 $m^2\ g^{-1}$) shows a faradaic pseudo-capacitance (217 F g^{-1}) which is dozens of electric double layer capacitance [2]. Besides, the SC of about 309 F g^{-1} displayed in curve (c) is far higher than (b) and it may be attributed to the increased MWCNTs@MnO_2 electrode conductivity in the presence of MWCNTs.

The above conclusions (Fig. 7) have been confirmed by EIS measurements performed on the three samples and the resulting Nyquist plots were displayed in Fig. 8. The impedance spectra are almost similar in form with a depressed semicircle in the high-to-medium frequencies region which is usually called Warburg semicircle [21,36] and the low-frequency straight line which is corresponding to ion diffusion in the electrode material. As shown in Fig. 8 (the inset plot magnified), the low frequency straight line of the MWCNTs@MnO_2 composite is almost vertical, indicating a good capacitive behavior. The measured impedance spectra can be fitted by using the software of Zsimpwin on the basis of the equivalent circuit consisting of R_s, a combination of the contact resistance of the active materials with substrate and the test cell to the apparatus, the ionic resistance of electrolyte, the intrinsic resistance of electrodes, R_{ct}, a charge-transfer resistance, C_{dl}, a double-layer capacitance and Z_w, Warburg impedance, presented in the inset of Fig. 8. R_{ct}, also called Faraday resistance, determines charging and discharging rate of supercapacitors, which is an extremely significant factor affecting the power density of a supercapacitor. R_{ct} obtained from the x-intercept of the Nyquist plots are measured to

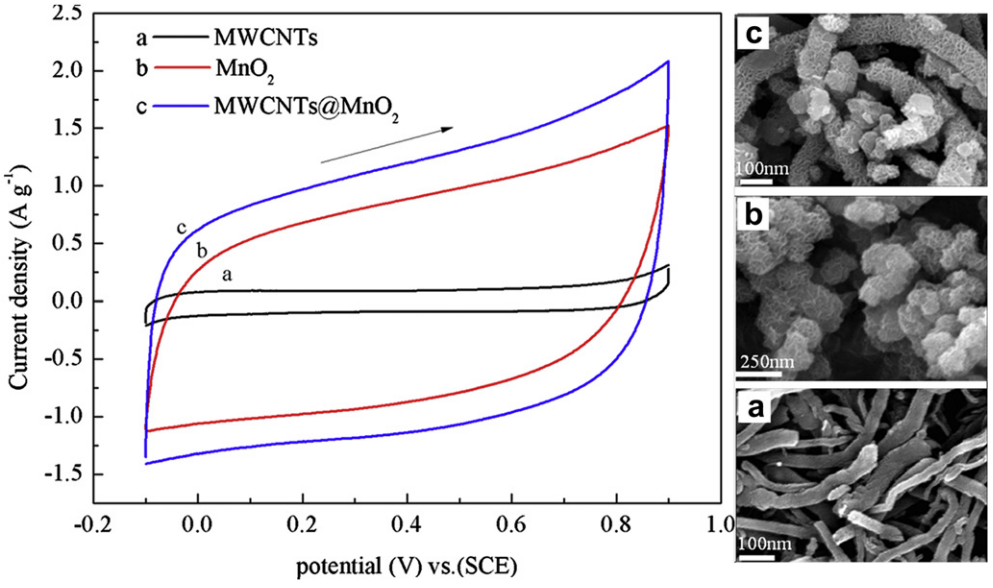

Fig. 7. CV curves at 5 mV s^{-1} in 0.5 M Na_2SO_4 solution and (the right insets) SEM images of as-prepared samples: (a) MWCNTs, (b) pristine MnO_2, and (c) MWCNTs@MnO_2.

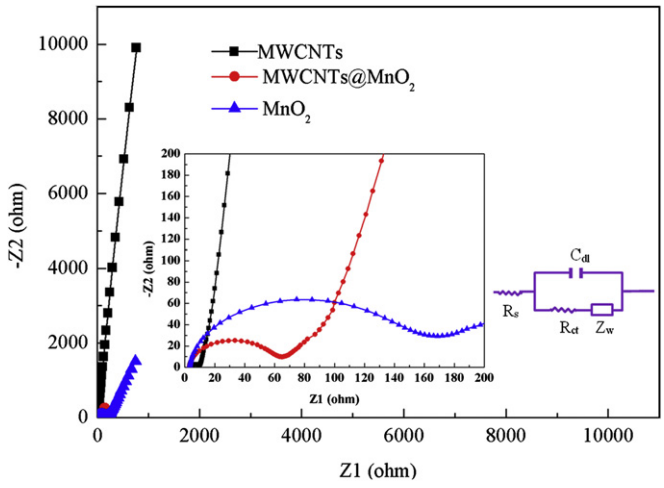

Fig. 8. Typical Nyquist impedance spectrum of MWCNTs@MnO_2, pristine MnO_2 and MWCNTs at open circuit potential (vs. SCE) within frequency range (0.01–10^5 Hz).

be 6 Ω, 60 Ω and 170 Ω for MWCNTs, MWCNTs@MnO_2, and pristine MnO_2, respectively. The gradually increased R_{ct} with the content of MnO_2 in the electrodes demonstrates that MWCNTs with good electrical conductivity can lower the charge-transfer resistance and thus improve the power density of a supercapacitor.

The long-term cycle stability is a very significant requirement for the practical applications of supercapacitors. The MWCNTs@MnO_2 electrode was subjected to an extended charge–discharge cycling at 5 A g^{-1} and the result was depicted in Fig. 9a. After 3500 cycles, 82.7% of SC was reserved, indicating the MWCNTs@MnO_2 core–shell structured materials bear excellent cycle stability. It has probably benefited from the MnO_2 nanoflakes growth round the MWCNTs electrochemically rather than a mechanical blending. The inset of Fig. 9a shows some representative charge–discharge curves. It can be seen that the curves reveal a highly linear and symmetric shape with small resistance drops, further confirming the excellent supercapacitive behavior and superior electrochemical reversibility. The SC and power density generated from the discharging curves were calculated to be 380 F g^{-1} and 11.28 kW kg^{-1}, which is relatively improved based on the results of the literatures. Such outstanding electrochemical performances demonstrate that the MWCNTs@MnO_2 composite can be a competitive candidate for supercacitors.

The rate capability is another criterion for practical applications. The constant current galvanostatic charge/discharge curves of the as-prepared MWCNTs@MnO_2 composite at different current densities between −0.1 and 0.9 V in 0.5 M Na_2SO_4 solution are shown in Fig. 9b. The specific capacitance obtained from the discharging curves is calculated to be 430 F g^{-1} by Eq. (2) at a low current density of 1 A g^{-1}. As the current density increasing to 25 A g^{-1}, the specific capacitance remains at 315 F g^{-1}. 73% of capacitance is retained when the current density changes from 1 A g^{-1} to 25 A g^{-1}. The excellent rate capability may be attributed to the enhanced conductivity of the electrode.

4. Conclusions

In-situ precipitation process to create nano-structured MWCNTs@MnO_2 for use as a highly capacitive and reversible electrode material is reported. The distinct uniform MnO_2 nanoflakes, with controlled particle size about 20 nm in diameter are obtained on MWCNTs with a large surface area. According to the results of the SEM, TEM, BET and a series of electrochemical techniques, the as-prepared MWCNTs@MnO_2 appear a mesoporous core–shell structure with a peak at 38 nm in diameter; the BET surface area of the

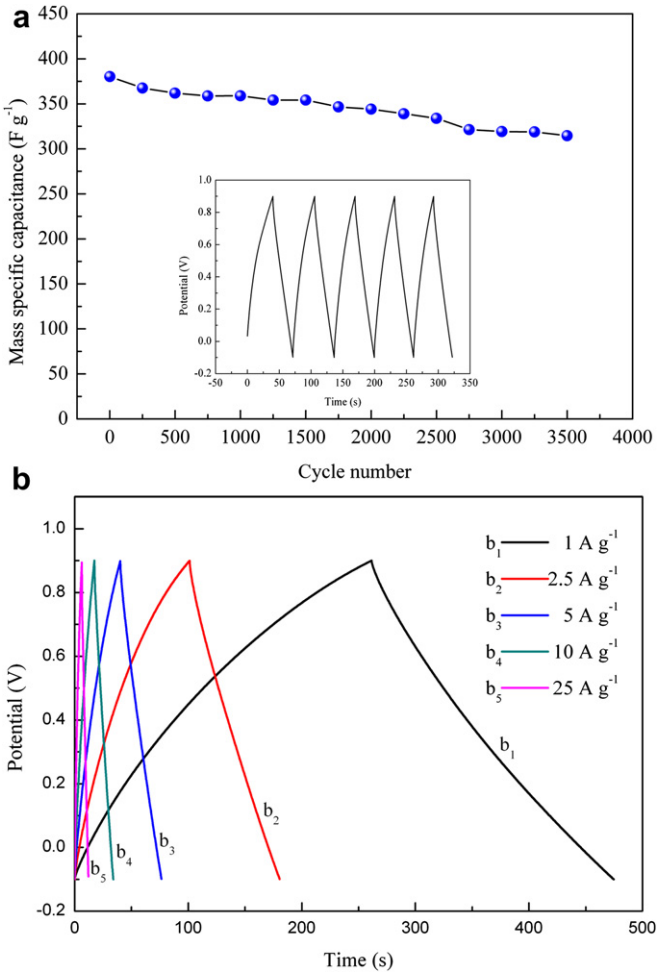

Fig. 9. (a) Long-term stability and (the inset) galvanostatic charge–discharge curves of symmetric cells of the MWCNTs@MnO_2 electrode at a current density of 5 A g^{-1} between −0.1 and 0.9 V in 0.5 M Na_2SO_4 solution; (b) galvanostatic charge–discharge curves of the MWCNTs@MnO_2 electrode at different current densities.

MWCNTs@MnO_2 can reach as high as 135.54 m^2 g^{-1} and the SC reaches up to 380 F g^{-1} at 5 A g^{-1} in 0.5 M Na_2SO_4 electrolyte. Long-term cycle stability test shows that the SC retention is still 82.7% after 3500 cycles at 5 A g^{-1}. The MWCNTs@MnO_2 shows superior electrochemical performance and excellent cycling stability as supercapacitor electrode materials. Compared with the results of the literatures, the performance of the MWCNTs@MnO_2 composites synthesized by co-precipitation method is significantly improved, and this MWCNTs@MnO_2 core–shell structured material will be a very promising supercapacitor electrode material.

Acknowledgment

This work was financially supported by Zhejiang major social development of major scientific and technological special projects (NO. 2010C13017).

References

[1] J. Chmiola, C. Largeot, P.L. Taberna, P. Simon, Y. Gogotsi, Science 328 (2010) 480–483.
[2] B.E. Conway, Electrochemical Supercapacitors, Kluwer-Plenum, New York, 1999.
[3] J.R. Miller, R.A. Outlaw, B.C. Holloway, Science 329 (2011) 1637–1639.
[4] J.X. Li, N. Wang, Y. Zhao, Y.H. Ding, L.H. Guan, Electrochem. Commun. 13 (2011) 698–700.

[5] Y.C. Chen, Y.K. Hsu, Y.G. Lin, Y.K. Lin, Y.Y. Horng, L.C. Chen, K.H. Chen, Electrochim. Acta 56 (2011) 7124–7130.
[6] D.Y. Zhai, B.H. Li, C.J. Xu, H.D. Du, Y.B. He, C.G. Wei, F.Y. Kang, J. Power Sources 196 (2011) 7860–7867.
[7] W.I. Jung, M. Nagao, C. Pitteloud, A. Yamada, R. Kanno, J. Power Sources 195 (2010) 3328–3332.
[8] W.F. Wei, X.W. Cui, W.X. Chen, D.G. Ivey, J. Power Sources 186 (2009) 543–550.
[9] M. Toupin, T. Brousse, D. Bélanger, Chem. Mater. 16 (2004) 3184–3190.
[10] Q. Cheng, J. Tang, J. Ma, H. Zhang, N. Shinya, L.C. Qin, Carbon 49 (2011) 2917–2925.
[11] X.F. Yang, G.C. Wang, R.Y. Wang, X.W. Li, Electrochim. Acta 55 (2010) 5414–5419.
[12] Q. Li, J.H. Liu, J.H. Zou, A. Chunder, Y.Q. Chen, L. Zhai, J. Power Sources 196 (2011) 565–572.
[13] C.J. Xu, B.H. Li, H.D. Du, F.Y. Kang, Y.Q. Zeng, J. Power Sources 180 (2008) 664–670.
[14] D.L. Yan, Z.L. Guo, G.S. Zhu, Z.Z. Yu, H.R. Xu, A.B. Yu, J. Power Sources 199 (2012) 409–412.
[15] M. Zhou, X. Zhang, L. Wang, J.M. Wei, L. Wang, K.W. Zhu, B.X. Feng, Mater. Chem. Phys. 130 (2011) 1191–1194.
[16] B.S. Ming, J.L. Li, F.Y. Kang, G.Y. Pang, Y.K. Zhang, L. Chen, J.Y. Xu, X.D. Wang, J. Power Sources 198 (2012) 428–431.
[17] H.J. Zheng, F.Q. Tang, M. Lim, A. Mukherji, X.X. Yan, L.Z. Wang, G.Q. Lu, J. Power Sources 195 (2010) 680–683.
[18] J. Yan, Z.J. Fan, T. Wei, W.Z. Qian, M.L. Zhang, F. Wei, Carbon 48 (2010) 3825–3833.
[19] J.G. Wang, Y. Yang, Z.H. Huang, F.Y. Kang, Electrochim. Acta 56 (2011) 9240–9247.
[20] R.R. Jiang, T. Huang, Y. Tang, J. Liu, L.G. Xue, J.H. Zhuang, A.S. Yu, Electrochim. Acta 54 (2009) 7173–7179.
[21] H.J. Wang, C. Peng, F. Peng, H. Yu, J. Yang, Mater. Sci. Eng. B 176 (2011) 1073–1078.
[22] S.B. Ma, K.W. Nam, W.S. Yoon, X.Q. Yang, K.Y. Ahn, K.H. Oh, K.B. Kim, J. Power Sources 178 (2008) 483–489.
[23] E. Raymundo-Pinero, V. Khomenko, E. Frackowiak, F. Beguin, J.Electrochem. Soc. 152 (2005) A229–A235.
[24] Z. Fan, J.H. Chen, B. Zhang, B. Liu, X.X. Zhong, Y.F. Kuang, Diam. Relat. Mater. 17 (2008) 1943–1948.
[25] H.J. Zheng, K. Wang, F.M. Zhao, F.Q. Tang, T.E. Rufford, L.H. Wang, C.N. Ma, Solid State Ionics 181 (2010) 1690–1696.
[26] S.L. Chou, J.Z. Wang, S.Y. Chew, H.K. Liu, S.X. Dou, Electrochem. Commun. 10 (2008) 1724–1727.
[27] F. Teng, S. Santhanagopalan, Y. Wang, D.D. Meng, J. Alloys Compd. 499 (2010) 259–264.
[28] W. Tang, Y.Y. Hou, X.J. Wang, Y. Bai, Y.S. Zhu, H. Sun, Y.B. Yue, Y.P. Wu, K. Zhu, R. Holze, J. Power Sources 197 (2012) 330–333.
[29] H.J. Zheng, F.Q. Tang, Y. Jia, L.Z. Wang, Y.C. Chen, M. Lim, L. Zhang, G.Q. Lu, Carbon 47 (2009) 1534–1542.
[30] H.J. Zheng, F.Q. Tang, M. Lim, T. Rufford, A. Mukherji, L.Z. Wang, G.Q. Lu, J. Power Sources 193 (2009) 930–934.
[31] L.Z. Zhang, J. Ma, X. Li, S.T. Wang, J. Environ. Sci. 21 (2009) 872–876.
[32] E.P. Barrett, L.G. Joyner, P.P. Halenda, J. Am. Chem. Soc. 73 (1951) 373–380.
[33] H.J. Wang, L.L. Zhu, S. Peng, F. Peng, H. Yu, J. Yang, Renew. Energy 37 (2012) 192–196.
[34] Q.T. Qu, L. Li, S. Tian, W.L. Guo, Y.P. Wu, R. Holze, J. Power Sources 195 (2010) 2789–2794.
[35] Y.P. Lin, C.B. Tsai, W.H. Ho, N.L. Wu, Mater. Chem. Phys. 130 (2011) 367–372.
[36] L. Wang, D.L. Wang, Electrochim. Acta 56 (2011) 5010–5015.